Deep-learning Based Ship-radiated Noise Suppression for Underwater Acoustic OFDM Systems

Lazar Atanackovic[†], Lutz Lampe[†], and Roee Diamant[§]

[†]Department of Electrical and Computer Engineering, University of British Columbia, Canada
[§]Department of Marine Technologies, University of Haifa, Israel
Corresponding author, email: *lazaratan@ece.ubc.ca*

***Abstract*—Interference due to ship-radiated noise in the underwater acoustic (UA) channel generates additive distortions that degrade wireless UA communications signals. Compressed sensing (CS) techniques are an approach used to estimate and suppress the impulsive components of ship-radiated noise for orthogonal frequency-division multiplexing (OFDM) systems by exploiting the null sub-carriers not used for data transmission. However, these CS-based estimation methods are constrained to estimating sparse signals and typically require slow iterative solvers. To combat these drawbacks, we propose a deep learning (DL) approach to structured signal recovery for estimating and mitigating the interfering effects of ship-radiated noise for OFDM systems. Our results indicate that the DL models, trained via publicly available long term acoustic data of shipping noise signals, produce measurable mitigation gains to the benchmark CS algorithms. In addition, we show the DL models outperform the benchmark CS estimation methods on new never before "seen" experimentally acquired ship-radiated noise data.**

***Index Terms*—Deep learning (DL), deep neural network (DNN), compressed sensing (CS), orthogonal frequency-division multiplexing (OFDM), ship-radiated noise.**

I. Introduction

Achieving high data rate and robust communications in the underwater acoustic (UA) channel continues to be a challenge due to a variety of factors [1]. The presence of multi-path effects, limited bandwidth, Doppler shifts, and numerous sources of interference are just some of the characteristics of the UA channel that contribute to producing the demanding channel conditions. Ship-radiated noise is one example of interference, found to carry impulsive characteristic [2] [3] that can be detrimental to high data rate UA communication systems. In this work, we focus on the challenge of suppressing the impulsive components and correlative structure of ship-radiated noise.

Orthogonal frequency-division multiplexing (OFDM) is a popular transmission technique utilized to handle the frequency selectivity present in the UA channel [4]. To combat against impulse noise interference in OFDM communication systems, compressed sensing (CS) based approaches for the estimation and suppression of impulse noise have been proposed [3] [5] [6]. These approaches take advantage of the null sub-carriers of the OFDM system to probe the impulsive interference, then provide an iterative CS estimate by exploiting the inherit sparsity of the impulse noise. The impulse noise estimate is then subtracted from the received data to reduce the overall level of degradation. However, the drawback of these CS-based impulse noise mitigation methods is that they require iterative solvers that may be too slow for real-time application. To this end, a deep learning (DL) approach that replaces the iterative CS recovery procedure with a trained deep neural network (DNN) may serve as a suitable alternative.

The field of communications has seen extensive success in using DL-based solutions, demonstrating measurable and advantageous results to traditional analytical approaches in areas such as physical layer transmitter and receiver design [7], channel estimation and signal detection [8], and communication networks [9]. In general, DL-based solutions accept slow off-line run-time during the training process to obtain significantly faster on-line application speeds compared to their respective counterpart approaches, thus desirable in many communication systems applications. The applications of DL in wireless communications have quickly extended into UA communications to handle the various non-linear distortions present in the UA channel. For instance, [10] offers a DL-based receiver for on-line channel estimation and equalization for single carrier UA communication systems. Likewise, channel estimation techniques via DL in multi-carrier UA OFDM systems have received significant research attention [11]–[13]. While [11] and [12] offer DL-based solution for channel estimation for UA OFDM systems, [13] is one of very few research works that suggest a DL-based method for handling impulse noise perturbations in the UA channel.

To the best of our knowledge, no research studies have investigated the applicability of DL-based approaches for mitigating the interfering effects of ship-radiated noise. However, various studies have suggested and shown the success of DL methods for ship classification and detection via acoustic signatures [14], [15]. This suggest that acoustic ship-radiated noise carries correlative structure that can be captured by DL models.

Recently, DL-based approaches for structured signal recovery from linearly and non-linearly sampled measurement have received attention in the domain of image processing [16] [17]

This work is supported by the NATO Science for Peace and Security Programme under grant G5293.

and have shown competitive recovery results to the counterpart CS methods. In [16], a linear stacked de-noising autoencoder (L-SDA) is employed to recover sets of original signals from their linearly sampled measurements. Moreover, the authors propose a non-linear stacked de-noising autoencoder (NL-SDA), which simultaneously learns a non-linear sampling procedure alongside the recovery stage, improving the overall recovery results. The use of convolutional neural networks (CNNs) in the setting of structured signal recovery presents similar recovery results also measurable to state-of-the-art CS methods [17]. The two key advantages of the DL recovery methods in contrast to the counterpart CS solvers are: (1) they do not rely on the sparsity of the signal of interest through linear transformation as do the CS methods, and (2) they trade off slow off-line run-time during the model training process for superior on-line run-time.

Motivated by the fact that ship-radiated noise carries correlative structure and due to the recent success and advantages of DL methods for structured signal recovery, we propose the use the existing DL models in the application of suppressing ship-radiated noise for UA OFDM systems. In the same manner as [3], we conduct a data driven study utilizing the Ocean Networks Canada (ONC) publicly available database of long-term acoustic shipping noise recordings [18]. In addition, we include experimentally acquired data to show the off-line trained DL models can scale to new never before "seen" sets of ship-radiated noise signals.

The rest of this manuscript is organized as follows. In Section II, we introduce the CS framework for sparse signal estimation, the OFDM system model, and the ONC and experimental data acquisition procedures. Section III outlines the general structures of the DNN models for structured signal recovery. Then, in Section IV, we present and discuss the numerical results for ship-radiated noise suppression via the DL-based approaches. Finally, we draw relevant conclusion that adhere from the numerical results in Section V.

II. Methodology and System Formulation

We consider the utilization of an OFDM system for the transmission and reception of data in the UA channel. Our aim is to exploit a partition of the OFDM system sub-carriers to probe, estimate, and then subtract out the ship-radiated noise interference from the received OFDM signal. In particular, we utilize the null sub-carriers of the OFDM system to sample the ship-radiated noise contributions from the received OFDM signal. The problem of estimating the ship-radiated noise interference can then be posed as a CS recovery problem [3]. In this section, we will introduce the CS framework for sparse signal estimation in OFDM systems that will serve as an underlying foundation for the DL-based structured signal recovery methods.

A. Compressed Sensing

CS is concerned with the problem of finding a solution to an undetermined linear system from a set of randomized measurements sampled far below the Nyquist rate, under the assumption that the solution is sparse [19]. Let us consider the linear system $\boldsymbol{y} = \boldsymbol{A}\boldsymbol{x} + \boldsymbol{n}$, where $\boldsymbol{A}$ is an $m \times K$ random measurement matrix, $\boldsymbol{y}$ is the $m \times 1$ measurement vector, $\boldsymbol{x}$ is $K \times 1$, $\boldsymbol{n}$ is additive white Gaussian noise (AWGN), and $m < K$. With the sparsity constraint enforced by the ℓ_1-norm, the CS recovery problem is formulated as

$$\begin{aligned} \underset{\boldsymbol{x}}{\textit{minimize}} \quad & \|\boldsymbol{x}\|_1 \\ \textit{subject to} \quad & \|\boldsymbol{y} - \boldsymbol{A}\boldsymbol{x}\|_2 \leq \epsilon \end{aligned} \tag{P1}$$

where the parameter ϵ is selected based on the measurement noise vector $\boldsymbol{n}$ [20]. The recovery procedure of (P1) is formally known as basis pursuit de-noise (BPDN) and is considered as a benchmark recovery algorithm for the remainder of this work.

B. OFDM System Model

Given N OFDM sub-carriers, we construct the $N \times N$ discrete Fourier transform (DFT) matrix $\boldsymbol{F}$. We define $\mathcal{S}$ as the set of data sub-carriers used for transmission and $\mathcal{S}^c$ as the set of null sub-carriers. Then, the partial DFT sampling matrix $\boldsymbol{F}_n$ is formed by selecting the rows of $\boldsymbol{F}$ from the set of null index locations defined in $\mathcal{S}^c$. The set of null sub-carrier locations $\mathcal{S}^c$ are chosen to some extent at random such that the reduced DFT measurement matrix $\boldsymbol{F}_n$ satisfies the restricted isometry property [21] in order to achieve greater reconstruction accuracy.

let us denote the received time domain OFDM signal as $\boldsymbol{z}$, which carries the data $\boldsymbol{d}$ and the additive ship-radiated noise interference $\boldsymbol{w}$. We probe the ship-radiated noise interference via the partial DFT sampling matrix, denoting the received signal as

$$\boldsymbol{r}' = \boldsymbol{F}_n\boldsymbol{z} = \boldsymbol{F}_n(\boldsymbol{d} + \boldsymbol{w}) \tag{1}$$

Following the CS framework, the ship-radiated noise interference $\boldsymbol{w}$ can be split into an impulse component $\boldsymbol{i}$ and AWGN component $\boldsymbol{\zeta}$. Then, with the knowledge that $\boldsymbol{F}_n\boldsymbol{d} = 0$, the received vector $\boldsymbol{r}'$ can be further simplified to

$$\begin{aligned} \boldsymbol{r} &= \boldsymbol{F}_n(\boldsymbol{i} + \boldsymbol{\zeta}) \\ &= \boldsymbol{F}_n\boldsymbol{i} + \tilde{\boldsymbol{\zeta}} \end{aligned} \tag{2}$$

where the pilot-data contribution has been subtracted from $\boldsymbol{r}'$ and $\boldsymbol{F}_n\boldsymbol{\zeta} = \tilde{\boldsymbol{\zeta}}$. Following from the result of equation (2) and with the assumption that the impulse noise $\boldsymbol{i}$ is sparse, we can formulate an estimate for the ship-radiated impulse noise component as

$$\begin{aligned} \underset{\boldsymbol{i}}{\textit{minimize}} \quad & \|\boldsymbol{i}\|_1 \\ \textit{subject to} \quad & \|\boldsymbol{r} - \boldsymbol{F}_n\boldsymbol{i}\|_2 \leq \epsilon \end{aligned} \tag{P2}$$

where (P2) is consistent with the form of BPDN defined by (P1).

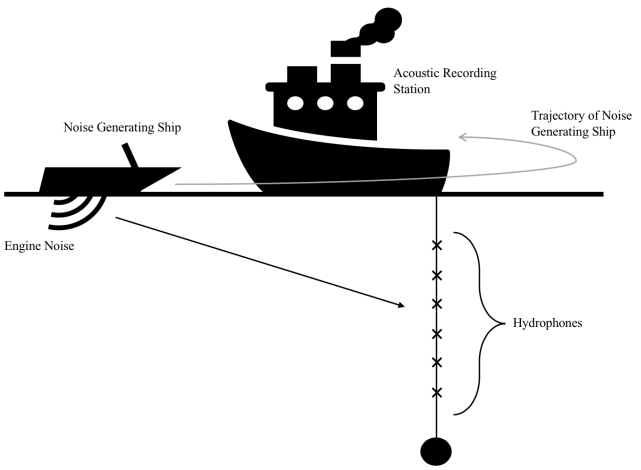

Fig. 1. Experimental set-up for acoustic acquisition of ship-radiated noise recordings.

C. Data Acquisition and Pre-processing

We collect the ONC data in an identical manner to the procedure outlined in [3, Section II-C]. In addition, we include experimental ship-radiated noise acoustic recordings collected through a set of sea trials off the coast of Caesarea, Israel, over a two day period of May 20^{th} and May 21^{st}, 2019. The experimentally acquired acoustic shipping noise recordings are used for further test validation of the DNN models for structured signal estimation.

The experimental acquisition set-up of the acoustic shipping noise recordings is presented in Fig 1. A linear array of 6 hydrophones placed at approximately equal spacing over 10 meters of length with the first hydrophone starting at a depth of approximately 15 meters is used. The "noise generating ship" follows an elliptical trajectory around the acoustic recording station which produces acoustic ship-radiated noise, as shown in Fig 1. The experimental acoustic recording acquisition procedure is outlined as follows:

1) With the "noise generating ship", we encircle the primary ship in a circular trajectory and begin the acoustic recording via the hydrophone array. We record via the hydrophone array for approximately 1 minute in duration.
2) The time of day of the acoustic recording, later used to filter and find relevant data files, is noted.

We repeat the above steps at several occasions to gather an assortment of acoustic ship-radiated noise recordings over the duration of the 2 day sea trial.

The ONC and experimental acoustic recordings are processed such that we can emulate signal reception of the OFDM system. We down-convert and low pass filter (LPF) the ONC and experimental shipping noise data. We consider high frequency (HF) and low frequency (LF) systems, outlined in Table I.

TABLE I
ACOUSTIC RECORDING PRE-PROCESSING FREQUENCY BANDS

	Center Frequency	Bandwidth	LPF Cut-off
Low Frequency	2 kHz	4 kHz	2 kHz
High Frequency	12 kHz	8 kHz	4 kHz

III. Deep Neural Networks for Structured Signal Estimation

We aim to utilize existing DL models, with the addition of complex DNN operations [22] and some augmentation to the model parameters, to realize ship-radiated noise estimation and mitigation. In particular, our primary goal is to learn a non-linear mapping to solve problem (P2) using the ONC shipping noise data set.

We consider three DL models for the structured signal recovery of ship-radiated noise in UA OFDM systems:

- The L-SDA [16] – a fully connected DNN.
- The NL-SDA [16] – a fully connected DNN.
- An implementation of the *Deep-inverse* model [17] – a CNN-based model for structured signal recovery.

Unlike the standard CS solvers, which only estimate the sparse components of the shipping interference signal, the DNN-based approaches also recover the correlative structures of the ship-radiated noise. Thus, we are able to achieve an estimate for the entire shipping noise signal $\boldsymbol{w}$ in addition to the impulsive components $\boldsymbol{i}$. The outputs of the L-SDA, NL-SDA, and the CNN models for structure signal recovery will yield an estimate $\hat{\boldsymbol{w}}$, and therefore the mitigated ship-radiated noise signal is reported as $\tilde{\boldsymbol{w}} = \boldsymbol{w} - \hat{\boldsymbol{w}}$.

For the remainder of this section, we introduce and describe the L-SDA, NL-SDA, and CNN models for the structured signal recovery of ship-radiated noise in terms of single real number networks. However, to handle the complex ship-radiated noise signals we use complex DNN operations [22]. The complex DNN models consist of two identical networks that are trained and evaluated in parallel that capture the mathematical dependencies between the real and imaginary components of the ship-radiated noise interference.

A. Stacked De-noising Autoencoder

Let us denote $\boldsymbol{x}$ as the 1024×1 complex input vector, $\boldsymbol{y}$ the $m \times 1$ sampled measurement vector, and $\boldsymbol{\Phi}$ as the $m \times 1024$ complex measurement matrix. The quantity of measurement points is denoted by m, where $m < 1024$. The goal is to achieve an estimate $\hat{\boldsymbol{x}}$ from the sampled measurement vector $\boldsymbol{y}$ by training a stacked de-noising autoencoder (SDA) that learns a non-linear mapping that is analogous to the CS recovery problem. An example of the general structure of a SDA is illustrated in Fig 2. Below we describe the individual implementations of the L-SDA and NL-SDA.

- **L-SDA**: In this implementation, the measurement matrix $\boldsymbol{\Phi}$ is fixed. In our case, $\boldsymbol{\Phi} = \boldsymbol{F_n}$, where $\boldsymbol{F_n}$ is the reduced DFT sampling matrix. We use the hyperbolic tangent function defined as $\tanh(z) = \frac{e^z - e^{-z}}{e^z + e^{-z}}$ at the

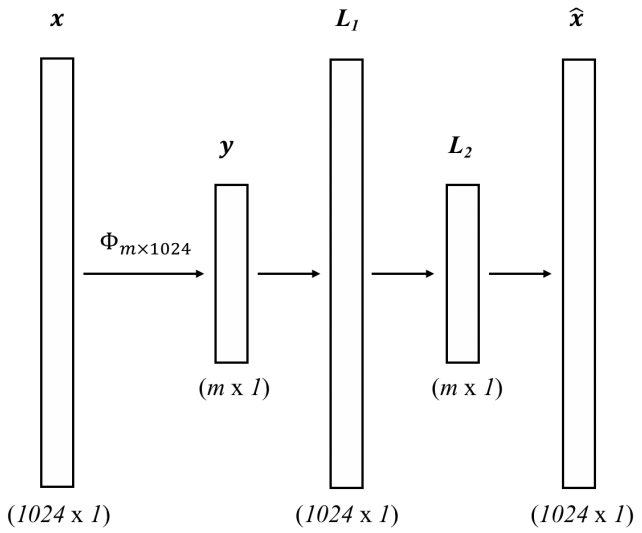

Fig. 2. Stacked de-noising autoencoder for structured signal recovery [16].

hidden layers, L_1 and L_2, as well as the output layer. The L-SDA learns a non-linear mapping from $\boldsymbol{y} = \boldsymbol{F_n x}$ and produces an estimate $\hat{\boldsymbol{x}}$.

- **NL-SDA**: Different from the L-SDA, this implementation learns the measurement paradigm defined by the matrix $\boldsymbol{\Phi}$ while simultaneously learning a non-linear mapping to estimate $\boldsymbol{x}$. This is advantageous to the L-SDA as the learned measurement procedure enables more efficient encoding of the input examples $\boldsymbol{x}$ compared to the reduced DFT sampling matrix. Similar to the L-SDA, the hyperbolic tangent activation function is used at the hidden layers, L_1 and L_2, the output layer, and additionally at the sampling layer, i.e. $\tanh(\boldsymbol{y}) = \tanh(\boldsymbol{\Phi x})$. Because the NL-SDA learns a new optimized sampling procedure that is not the reduce DFT matrix, it does not serve as a realizable implementation for OFDM systems. Therefore, we use the NL-SDA as a upper benchmark on the performance of the L-SDA with the reduce DFT measurement matrix.

To aid and accelerate the training procedure, we also include the use of batch normalization layers, placed after the fully connected layers and prior to the activation layers.

B. Convolutional Neural Network

Different from the SDA implementations, the CNN for structured signal recovery uses convolutional layers to reduce the overall quantity of parameters for training while taking advantage of the natural structures of the input signals in order to achieve an accurate estimate $\hat{\boldsymbol{x}}$. Fig 3 illustrates our CNN model architecture that stems from the *Deep Inverse* model proposed by [17]. Different from *Deep Inverse*, our model operates in one dimension and uses less feature maps at each hidden layer, however the principle of first achieving a pseudo-estimate $\tilde{\boldsymbol{x}} = \boldsymbol{\Phi}^H \boldsymbol{y}$ from the linearly samples vector $\boldsymbol{y}$ remains the same.

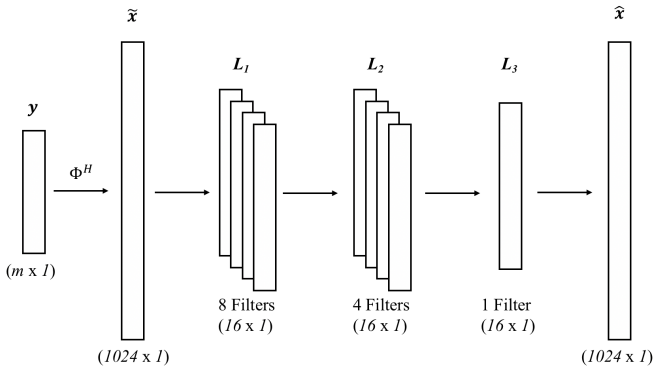

Fig. 3. Convolutional DNN for structured signal recovery [17].

Alike the SDA implementations we utilize the hyperbolic tangent activation function at the output of hidden layers L_1, L_2, and L_3, as well as at the output layer. Batch normalization layers are also included between the outputs of each hidden layer and the activation layer to facilitate for a fast and robust training phase. Each of the hidden layers L_1, L_2, and L_3 use a 16×1 convolutional filter and preserve the input size of the previous layers.

IV. Numerical Results

A. Training and Testing Data

We use the ONC ship-radiated noise data set to train and test the DNN models for structured signal recovery and use the experimentally acquired ship-radiated noise data for further evaluation of the ONC trained DNN models. The evaluation of the DNN models using the experimental data set serves to demonstrate how the ONC trained DNN models scale to new never before "seen" ship-radiated noise signals, acquired under entirely different conditions compared to the ONC shipping noise data. The ONC test data and experimental ship-radiated noise data are used only in the testing stages of the DNN models, thus have no influence on the training of the DNNs.

To aid in the training procedure, each input data example vector and output data label vector is normalized between $[-1,\ 1]$, thus after the estimation step we must re-normalize the estimate $\hat{\boldsymbol{x}}$ to have a generalized framework for estimating any ship-radiated noise signal via the DNN models. Let $\boldsymbol{X}'$ denote the $n \times N$ complex example matrix of ship-radiated noise signals and $\boldsymbol{Y}'$ the $n \times m$ sampled example matrix of ship-radiated noise signals, where n is the number of shipping noise signal examples, $N = 1024$ the number of OFDM system sub-carriers, and m the quantity of null sub-carrier sampling points. Then, for each example i, the per-signal data normalization are defined as

$$\boldsymbol{X}_i = \frac{1}{\sqrt{2}} \frac{\boldsymbol{X}'_i}{\max\{|\boldsymbol{X}'_i|\}} \tag{3}$$

$$\boldsymbol{Y}_i = \frac{1}{\sqrt{2}} \frac{\boldsymbol{Y}'_i}{\max\{|\boldsymbol{Y}'_i|\}} \ . \tag{4}$$

After the estimation stage of the DNN models, re-normalization of the output is required to conserve the original amplitudes of the ship-radiated noise signals. For the NL-SDA, this is trivial as we reverse the process of equation (3). However, for the L-SDA and CNN methods, we use the the sampled ship-radiated noise vectors to re-normalize the estimated output. Denoting the $n \times N$ complex estimate matrix of ship-radiated noise signals as $\hat{\boldsymbol{X}}$, the re-normalization of estimated output vector i is defined as

$$\hat{\boldsymbol{X}}_i' = \hat{\boldsymbol{X}}_i \frac{2\sqrt{2}}{\mathbb{E}[|\boldsymbol{Y}_i'|]} = \hat{\boldsymbol{X}}_i K \ . \tag{5}$$

The matrix $\boldsymbol{Y}'$ consists of the DFT sampled examples of $\boldsymbol{X}'$, i.e. $\boldsymbol{Y}'$ is a matrix containing the Fourier transformed ship-radiated noise signals at the null sub-carrier indices. Therefore, we use the spectral magnitude information provided from $\boldsymbol{Y}'$ of the sampled ship-radiated noise signals to estimate a re-normalization factor K that re-normalizes $\hat{\boldsymbol{X}}_i$ to $\hat{\boldsymbol{X}}_i'$.

The L-SDA, NL-SDA, and CNN models utilize different variants of training and testing sets. Let us denote $\mathcal{D}_{train} = \{\text{train data examples, train data labels}\}$ and $\mathcal{D}_{test} = \{\text{test data examples, test data labels}\}$ as the training and testing sets, respectively. Then, for each DNN model, we can define the individual training and testing sets:

- **L-SDA:** $\mathcal{D}_{train} = \{\boldsymbol{Y}_{train},\ \boldsymbol{X}_{train}\}$ and $\mathcal{D}_{test} = \{\boldsymbol{Y}_{test},\ \boldsymbol{X}_{test}\}$.
- **NL-SDA:** $\mathcal{D}_{train} = \{\boldsymbol{X}_{train},\ \boldsymbol{X}_{train}\}$ and $\mathcal{D}_{test} = \{\boldsymbol{X}_{test},\ \boldsymbol{X}_{test}\}$.
- **CNN:** $\mathcal{D}_{train} = \{\boldsymbol{F_n}^H \boldsymbol{Y}_{train},\ \boldsymbol{X}_{train}\}$ and $\mathcal{D}_{test} = \{\boldsymbol{F_n}^H \boldsymbol{Y}_{test},\ \boldsymbol{X}_{test}\}$.

We consider OFDM systems with $m = 256$ and $m = 128$ null sub-carriers, corresponding to the sampling ratios $m/n = 25\%$ and $m/n = 12.5\%$, and train DNN models for each case, respectively.

All three models are trained using the momentum based RMSprop optimizer and the mean squared error (MSE) loss function. For the L-SDA and NL-SDA, the learning rate is set to 0.0001 and the models are trained over 200 epochs. For the CNN model, the learning rate is set to 0.001 and the model is trained over 50 epochs. The DNN model weights for all cases are initialized with a standard normal. The overall HF train and test set sizes are 23040 and 5760, respectively. The LF data set is lesser in size compared to the HF data set, thus we include one-dimensional translation augmented versions of the pre-processed shipping noise signals to increase the LF data set size by a factor of 4. The LF train and test set sizes are 51321 and 5703, respectively. The training procedure uses a mini-batch size of 128 examples and the training set examples are randomly permuted at the start of every epoch to aid the training procedure convergence of the DNN models.

B. ONC Data Noise Suppression

We evaluate noise mitigation performance for the L-SDA, NL-SDA, and CNN methods by considering the per OFDM symbol ship-radiated noise variance σ^2 of the mitigated and original shipping noise signals from the ONC test data set. We compare the mitigation capabilities of the DNN models to BPDN and an idealistic GM-GAMP [3] implementation. In this setting, ideal GM-GAMP estimates the GMM parameters from the true ship-radiated noise signals prior to the estimation phase. In realistic applications, the full noise signals are unknown, thus the aforementioned GM-GAMP implementation is an idealistic approach. We plot the empirical cumulative distribution functions (CDFs) for the HF and LF systems and report the relative noise cancellation gains for the 90% and 99% strongest noise.

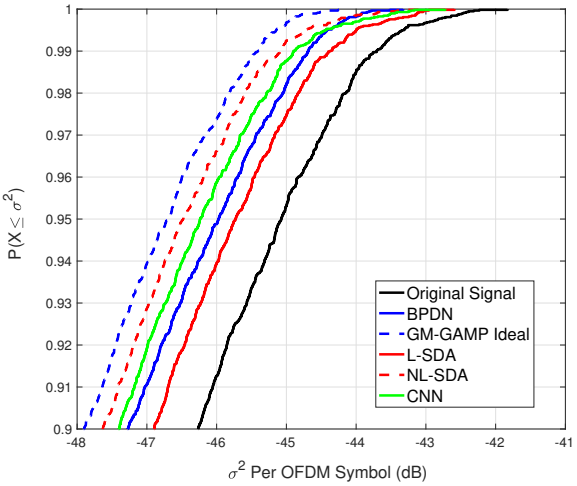

Fig. 4. Per-OFDM symbol noise variance of original and mitigated ship-radiated noise signals using 25% null sub-carriers sampling for HF-ONC test data set.

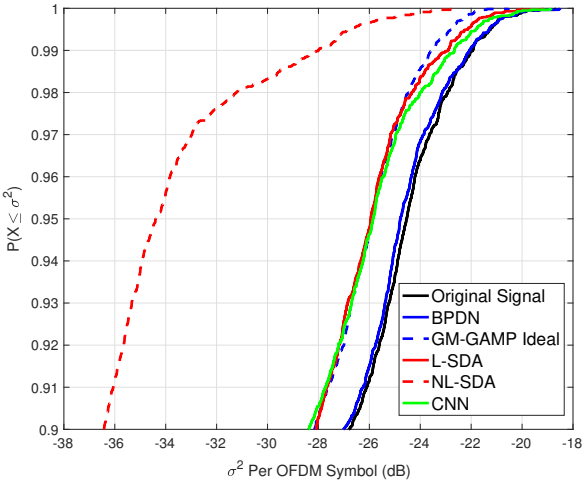

Fig. 5. Per-OFDM symbol noise variance of original and mitigated ship-radiated noise signals using 25% null sub-carriers sampling for LF-ONC test data set.

Fig 4 and Fig 5 show the per OFDM symbol noise variance of the respective method mitigated and original ship-radiated noise signals for the HF and LF systems, respectively. From Fig 4 It is visible that the NL-SDA and CNN methods achieve

TABLE II
RELATIVE MITIGATION GAIN OF SHIP-RADIATED NOISE WITH 25 % NULL SUB-CARRIER SAMPLING VIA THE DL-BASED ESTIMATION METHODS.

High Frequency					
$P(X > \sigma^2)$	BPDN	GM-GAMP	L-SDA	NL-SDA	CNN
0.1	1.01 dB	**1.64 dB**	0.63 dB	1.37 dB	1.14 dB
0.01	0.97 dB	**1.70 dB**	0.66 dB	1.38 dB	1.16 dB
Low Frequency					
$P(X > \sigma^2)$	BPDN	GM-GAMP	L-SDA	NL-SDA	CNN
0.1	0.26 dB	1.40 dB	1.33 dB	**9.67 dB**	1.64 dB
0.01	0.13 dB	1.65 dB	0.98 dB	**6.05 dB**	0.73 dB

TABLE III
RELATIVE MITIGATION GAIN OF SHIP-RADIATED NOISE WITH 12.5 % NULL SUB-CARRIER SAMPLING VIA THE DL-BASED ESTIMATION METHODS.

High Frequency					
$P(X > \sigma^2)$	BPDN	GM-GAMP	L-SDA	NL-SDA	CNN
0.1	0.20 dB	**0.72 dB**	0.19 dB	0.54 dB	0.53 dB
0.01	0.22 dB	**0.87 dB**	0.26 dB	0.61 dB	0.63 dB
Low Frequency					
$P(X > \sigma^2)$	BPDN	GM-GAMP	L-SDA	NL-SDA	CNN
0.1	−0.48 dB	−0.08 dB	0.50 dB	**7.50 dB**	0.28 dB
0.01	−0.09 dB	−0.05 dB	0.41 dB	**5.74 dB**	0.14 dB

measurable shipping noise mitigation to ideal GM-GAMP and outperform the BPDN algorithm for the HF system. Likewise, Fig 5 illustrates the superior mitigation gains of the NL-SDA in the LF band system. This is likely due to the increased correlative structure that exists in LF ship-radiated noise which the NL-SDA can learn to estimate. In contrast, HF ship-radiated noise contains a greater quantity of occurrences of random impulsive agitations that are more challenging to capture via the DNN models. Thus, the NL-SDA yields significantly improved mitigation gains for LF ship-radiated noise relative to HF ship-radiated noise. In addition, the L-SDA and the CNN methods outperform BPDN and closely match the mitigation performance of the ideal GM-GAMP algorithm in the LF band system.

Tables II and III present the relative mitigation gains for the 90% and 99% strongest noise for the cases of using 256 and 128 null sub-carriers of the total 1024 available sub-carriers, respectively. Tables II and III give a more precise presentation of ship-radiated noise mitigation capabilities of the respective approaches that are shown in Fig 4 and Fig 5.

The results suggest that the CNN method achieves measurable mitigation gains to the ideal GM-GAMP algorithm for ONC ship-radiated noise data, but with superior run-time performance as no iterative solvers are required. In terms of real-time applications, the superior run-time performance of the CNN method for ship-radiated noise suppression is a desirable trait. Therefore, in cases where high mitigation gains are desirable, GM-GAMP would serve as the algorithm of choice, but in cases where high run-time speed is required, the CNN mitigation method would suit as a better alternative.

The L-SDA method for ship-radiated noise mitigation never achieves the upper performance bound determined by the NL-SDA. This indicates that the bottleneck for the DNN approaches for shipping noise mitigation in UA OFDM systems is the reduced DFT sampling matrix. In the case such as the NL-SDA, the learned sampling procedure leads to improved mitigation results compared to the L-SDA and CNN approaches in the HF systems where shipping noise is more sparse. However, in the LF band system where ship-radiated noise is highly correlative, the NL-SDA shows superior mitigation gains to all other approaches, including the L-SDA which is approximately $5-9$ dB short in mitigation capability to the NL-SDA. This result demonstrates the power of the DNN-based methods for ship-radiated noise estimation and suppression, but standard OFDM systems that require the reduced DFT sampling matrix constrain the performance of the DNN-based approaches.

From Tables II and III, it is also visible that the CS-based methods, BPDN and ideal GM-GAMP, achieve higher mitigation gains for the 99% strongest noise relative to the 90% strongest noise. This is consistent to the basis of the CS-based algorithms, as the 99% strongest noise pertains to more impulsive (sparser) noise contributions. Moreover, we see the DNN-based approaches yield improved mitigation gains for the 90% strongest noise compared to the 99% strongest noise. This is also consistent with our expectations as the 90% strongest noise is less impulsive and carries increased correlative structure relative to the 99% strongest noise. This result suggest that some form of a hybrid approach that utilizes an iterative sparsity-based estimator and a DNN model in parallel could achieve improved ship-radiated noise mitigation capabilities.

C. Experimental Data Noise Suppression

After acquiring various experimental ship-radiated noise recordings we identify the acoustic hydrophone recordings with the most prominent shipping noise and no interference from other noise sources present during the sea trials. Two

TABLE IV
MSE BETWEEN ESTIMATED AND ORIGINAL EXPERIMENTAL SHIP-RADIATED NOISE SIGNALS USING 25% NULL SUB-CARRIER SAMPLING.

Ship Noise Data	**Estimation Method**				
	BPDN	GM-GAMP	L-SDA	NL-SDA	CNN
HF-EXP1	2.1E−6	1.7E−6	2.0E−6	1.6E−6	**1.0E-6**
HF-EXP2	3.0E−6	2.6E−6	3.0E−6	2.5E−6	**1.6E-6**
LF-EXP1	6.6E−5	5.4E−5	2.8E−4	5.2E−5	**1.2E-5**
LF-EXP2	6.9E−5	5.5E−5	2.7E−4	5.6E−5	**1.3E-5**

experimental recordings, both approximately one minute in length, are identified and considered for analysis:

- **Acoustic recording 1**: Date: May 20th, Time: 15:52 – Label: EXP1
- **Acoustic recording 2**: Date: May 20th, Time: 15:53 – Label: EXP2

Table IV presents the MSE results between the estimated and the actual experimental shipping noise signals using the BPDN algorithm, the ideal GM-GAMP implementation, and the three DNN models trained via the ONC data set. It is visible from Table IV that the CNN model for ship-radiated noise estimation outperforms all other methods on the experimental data in both HF and LF systems. This result suggests that the experimental ship-radiated noise signals contain similar correlative structure present in the ONC shipping noise data that is well captured by the convolutional filters of the CNN model. Thus, the CNN model is able to recover the experimental ship-radiated signals with better accuracy compared to BPDN and the ideal GM-GAMP implementation.

Overall the results indicate that the CNN method for ship-radiated noise cancellation scales best to new shipping noise instances that adhere from a source different from the ONC data set. This further confirms the shipping noise mitigation capabilities of the CNN method compared to ideal GM-GAMP, with the key advantage of superior run-time speed for noise cancellation.

V. CONCLUSION

In this paper, we introduced the DL-based approaches for ship-radiated noise cancellation in UA OFDM systems formulated under the CS noise estimation framework. The DL methods were evaluated in terms the per OFDM symbol noise variance shipping noise cancellation gains. The empirical results for the noise cancellation capabilities of the DNN-based approaches for ship-radiated noise suggest the CNN-based method for structured signal recovery is suitable as an alternative approach for the GM-GAMP and BPDN algorithms. This is particularly the case in the LF band system where ship-radiated noise exhibits increased correlative structure compared to the HF band system. In addition, the empirical mitigation results of the NL-SDA suggest that the bottleneck for achieving higher cancellation gains of ship-radiated noise in UA OFDM systems is the reduced DFT sampling procedure. Finally, we have demonstrated that the CNN model for ship-radiated noise cancellation scales best to newly never before seen experimental shipping noise signals. This is visible from the experimental results, where the CNN-based approach outperforms all other cancellation methods.

ACKNOWLEDGMENT

The authors would like to thank Ocean Networks Canada for providing the shipping noise data and accompanying help in using it.

REFERENCES

[1] M. Stojanovic and J. Preisig, "Underwater acoustic communication channels: Propagation models and statistical characterization," *IEEE Communications Magazine*, vol. 47, no. 1, pp. 84–89, 2009.

[2] T. Eggen, "Phase coherent communication in the presence of ship noise," in *Proceedings of OCEANS-Providence*, vol. 2. IEEE, 2000, pp. 1433–1436.

[3] L. Atanackovic, R. Zhang, L. Lampe, and R. Diamant, "Statistical shipping noise characterization and mitigation for underwater acoustic communications," in *Proceedings of OCEANS-Marseille*. IEEE, 2019, pp. 1–7.

[4] B. Pranitha and L. Anjaneyulu, "Review of research trends in underwater communications - A technical survey," in *Proceedings of the International Conference on Communication and Signal Processing*. IEEE, 2016, pp. 1443–1447.

[5] P. Chen, Y. Rong, S. Nordholm, Z. He, and A. J. Duncan, "Joint channel estimation and impulsive noise mitigation in underwater acoustic OFDM communication systems," *IEEE Transactions on Wireless Communications*, vol. 16, no. 9, pp. 6165–6178, 2017.

[6] S. Wu, S. Wang, Z. He, K. Niu, and Y. Rong, "An Approximate Message Passing Algorithm for Channel and Impulsive Noise Estimation in Underwater Acoustic OFDM Systems," in *Proceeding of OCEANS-Marseille*. IEEE, 2019, pp. 1–5.

[7] T. O'Shea and J. Hoydis, "An introduction to deep learning for the physical layer," *IEEE Transactions on Cognitive Communications and Networking*, vol. 3, no. 4, pp. 563–575, 2017.

[8] H. Ye, G. Y. Li, and B.-H. Juang, "Power of deep learning for channel estimation and signal detection in OFDM systems," *IEEE Wireless Communications Letters*, vol. 7, no. 1, pp. 114–117, 2017.

[9] C. Zhang, P. Patras, and H. Haddadi, "Deep learning in mobile and wireless networking: A survey," *IEEE Communications Surveys & Tutorials*, vol. 21, no. 3, pp. 2224–2287, 2019.

[10] Y. Zhang, J. Li, Y. V. Zakharov, J. Li, Y. Li, C. Lin, and X. Li, "Deep learning based single carrier communications over time-varying underwater acoustic channel," *IEEE Access*, vol. 7, pp. 38 420–38 430, 2019.

[11] Y. Zhang, J. Li, Y. Zakharov, X. Li, and J. Li, "Deep learning based underwater acoustic OFDM communications," *Applied Acoustics*, vol. 154, pp. 53–58, 2019.

[12] R. Jiang, X. Wang, S. Cao, J. Zhao, and X. Li, "Deep neural networks for channel estimation in underwater acoustic OFDM systems," *IEEE Access*, vol. 7, pp. 23 579–23 594, 2019.

[13] Z. Chen, Z. He, K. Niu, and Y. Rong, "Neural network-based symbol detection in high-speed ofdm underwater acoustic communication," in *Proceedings of the 10th International Conference on Wireless Communications and Signal Processing*. IEEE, 2018, pp. 1–5.

[14] M. Thomas, F. Lionel, and D.-P. Laurent, "Propeller noise detection with deep learning," in *Proceedings of the International Conference on Acoustics, Speech and Signal Processing-Barcelona*. IEEE, 2020, pp. 306–310.

[15] S. Shen, H. Yang, X. Yao, J. Li, G. Xu, and M. Sheng, "Ship type classification by convolutional neural networks with auditory-like mechanisms," *MDPI Sensors*, vol. 20, no. 1, p. 253, 2020.

[16] A. Mousavi, A. B. Patel, and R. G. Baraniuk, "A deep learning approach to structured signal recovery," in *Proceeding of the 53rd Annual Allerton Conference on Communication, Control, and Computing*. IEEE, 2015, pp. 1336–1343.

[17] A. Mousavi and R. G. Baraniuk, "Learning to invert: Signal recovery via deep convolutional networks," in *Proceedings of the International Conference on Acoustics, Speech and Signal Processing*. IEEE, 2017, pp. 2272–2276.

[18] Ocean Networks Canada, "Search hydrophone data," January 2016, https://data.oceannetworks.ca/SearchHydrophoneData.
[19] E. Candès and M. Wakin, "An introduction to compressive sampling," *IEEE Signal Processing Magazine*, vol. 25, no. 2, pp. 21–30, 2008.
[20] E. Candes, J. Romberg, and T. Tao, "Stable signal recovery from incomplete and inaccurate measurements," *Communications on Pure and Applied Mathematics: A Journal Issued by the Courant Institute of Mathematical Sciences*, vol. 59, no. 8, pp. 1207–1223, 2006.
[21] E. Candès, "The restricted isometry property and its implications for compressed sensing," *Comptes rendus mathematique*, vol. 346, no. 9-10, pp. 589–592, 2008.
[22] C. Trabelsi, O. Bilaniuk, Y. Zhang, D. Serdyuk, S. Subramanian, J. F. Santos, S. Mehri, N. Rostamzadeh, Y. Bengio, and C. Pal, "Deep complex networks," in *Proceedings of the International Conference on Learning Representations*, 2018.